International Journal of Nanoelectronics and Materials
IJNeaM
ISSN 1985-5761 | E-ISSN 2232-1535

Incoloy 800HT Weldolet Integrity in Hot Collector: Replica Testing Insights

Nur Farhana Hayazi[a,*], Ku Adri Azhan Ku Mohamad[a], Junaidi Che Halim[a] and Shaiful Rizam Shamsudin[b]

[a]*Surface Technology Special Interest Group, Faculty of Chemical Engineering and Technology, Universiti Malaysia Perlis (UniMAP), Arau, Perlis, Malaysia*
[b]*Faculty of Mechanical Engineering and Technology, Universiti Malaysia Perlis (UniMAP), Arau, Perlis, Malaysia*
**Corresponding author. Tel.: +604-9798751; fax: +604-9798755; e-mail: farhanahayazi@unimap.edu.my*

ABSTRACT

In this paper, the integrity assessment of Primary Reformer's hot collector weldolet in the fertilizer plant was conducted. It aims to discuss the findings of the relevant weldolet weldments which include dye penetrant test ultrasonic test, in-situ field metallography (replication), hardness measurements and rectification measures. The first step of the steam reforming process takes place in the Primary Reformer, where preheated hydrocarbon and steam mixture is passed downwards through vertical tubes containing catalyst. The hot gas that exited from the catalyst tubes is termed reformed gas and will enter two headers, namely hot and cold collectors. From then, the reformed gas will transform into raw ammonia synthesis gas after undergoing several processes. The facility was commissioned in 2006 and is still in operation. During the Plant Turnaround in 2022, the Primary Reformer's hot collector weldolet component is categorised as high nickel content material, commercially known as Incoloy 800HT, was detected with circumferential crack at several locations. The operating temperature of the weldolet is 811^{0}C. The observed damage mechanism of the crack was "Aged Phenomenon". However, at four locations of the weldments, further dye penetrant test (DPT) and metallurgical testing using replica test had observed sigma phase microstructure which is related to sigma phase embrittlement (SPE) without any creep cavity observed. Finally, both occurrences were reported and reviewed.

Keywords: *Primary reformer, Hot collector weldolet, Aging phenomena, Sigma phase embrittlement, Integrity assessment*

1. INTRODUCTION

The primary reformer plays a pivotal role in ammonia production, facilitating the conversion of hydrocarbons and steam into ammonia-rich synthesis gas. An essential component of this system is the hot collector weldolet, which is responsible for distributing reformed gases. Extreme conditions, including elevated temperatures and high-pressure operation, make this weldolet susceptible to wear and degradation over time [1].

Ammonia production is a critical industrial process that necessitates uninterrupted and efficient operation. Failures in components such as the hot collector weldolet can lead to unscheduled downtimes, reduced productivity, and potential safety hazards. Therefore, a comprehensive assessment of the weldolet's integrity becomes imperative to ensure the continued and reliable functioning of the primary reformer [2].

This paper explores the inspection and evaluation of the hot collector weldolet's condition, aiming to identify potential issues, such as corrosion, cracking, or other forms of degradation. By shedding light on the weldolet's structural integrity and wear characteristics, this study seeks to contribute to the maintenance and safety protocols of ammonia production plants, emphasizing the significance of periodic assessments to prevent loss of primary containment.

The subject of this exploration investigates the phenomenon of aging in heat-resistant steel during the occurrence of creep rupture. The aging process unfolds as a result of the prolonged exposure of the material to elevated temperatures and the application of mechanical stress. This phenomenon has significant ramifications, notably within industries characterized by high- temperature environments and mechanical demands, such as power generation and petrochemical processing.

The manifestation of aging during creep rupture primarily manifests through three distinct processes: carbide precipitation, carbide coarsening, and carbide transformation [3]. These intricate transformations are intrinsic to the aging phenomenon and significantly influence the mechanical properties and structural integrity of the heat-resistant steel. Carbide precipitation involves the formation of carbide particles within the material's microstructure, a consequence of the segregation of carbon and alloying elements. Subsequently, as aging proceeds, carbide coarsening ensues, resulting in the enlargement of pre-existing carbide particles. This coarsening phenomenon diminishes the material's resistance to deformation and rupture, accentuating its vulnerability to creep rupture. Additionally, carbide transformation contributes to aging by introducing changes in the composition and structure of carbides, which can significantly affect the material's strength and ductility, potentially leading to embrittlement. Understanding the complexities of aging

in heat- resistant steel during creep rupture, particularly the interplay of carbide precipitation, coarsening, and transformation, holds paramount importance [3, 4]. It is crucial for ensuring safety, optimising performance, guiding engineering decisions, and improving cost efficiency in high-temperature applications.

The integrity assessment of failure analysis is a crucial endeavor in various industries and engineering disciplines. Understanding the causes and mechanisms behind failures is essential for ensuring the reliability, safety, and performance of various systems, structures, and components. Failure analysis systematically investigates why and how materials, products, or systems malfunction, leading to undesirable outcomes. Failures can have far- reaching consequences, from compromising the structural integrity of bridges and buildings to causing safety hazards in industrial processes.

Integrity assessment through failure analysis aims to identify the root causes of failures, evaluate their implications, and develop strategies to prevent similar incidents in the future. The ultimate objective is to mitigate risks and prevent similar incidents and drive advancements in predictive maintenance and materials engineering. This will enhance the reliability, safety, and efficiency of industrial systems, contributing to significant cost savings and extending the lifespan of critical assets.

2. METHODOLOGY

Four locations of circumferential cracks at the hot collector weldolet to outlet hairpin weldment were found with rejectable indication by the dye-penetrant method. The observation of circumferential crack was found in the year 2016 after 10 years of service. The remedial actions to overcome the issue were defect removal, weld build-up and solution annealing. The planned permanent solution to this matter in the following turnaround in 2019 was to replace the primary reformer's hot collector with a new one. Hence, the reformer hot collector that had been in service for 9 years was used to conduct an on-site in-situ replication investigation was discussed in this paper. Full details on the chronology of the hot collector weldolet to outlet hairpin weldment are listed in Table 1. The Primary Reformer's hot collector weldolet component is commercially known as Incoloy 800HT or was sometimes named Alloy 800HT.

Chemical composition analysis was also performed beforehand. Then, when the dye-penetrant method was completed, the integrity assessment proceeded with in-situ replication works and hardness measurements on the joint. The work was carried out on the weldment which consists of base metal (BM), heat affected zone (HAZ) and weld deposit (WELD). Sample preparation for replication (in-situ field metallography) was conducted according to ASTM E1351-01(2020) [5]. Standard practice for producing and evaluating field metallographic replicas was used according to the VGB Standard (VGB-S-517-00-2014- 11-DE-EN) [6]. At the same time, the hardness measurements were conducted according to the work procedure of portable hardness testing by ultrasonic contact impedance (UCI) method. These hardness measurements were conducted using a Kräutkrämer, Microdur MIC 10 equipment. Each identified replicated location was ground, polished and etched with 10% oxalic acid.

The replication work and hardness measurement were conducted to determine if any degradation in material properties had occurred due to exposure to high temperature and pressure. The evaluation and interpretation of the microstructure on replication works were carried out based on the same code and class as described in Tables 2 and 3. The assessment of rating classes based on the results of the replica investigation is a crucial step in understanding the condition and integrity of a material, particularly in the context of Incoloy 800HT (hot collector weldolet) and similar alloys. This replica investigation involves creating a duplicate or replica of the material's microstructure, allowing for detailed examination under a microscope. This process assesses the extent of various microstructural changes, such as sensitization and carbide precipitation, which can affect the material's performance and longevity.

Table 1 Chronology of the hot collector weldolet to outlet hairpin weldment throughout the 9 years of service

Year	Observation
2006	Component starts commissioning.
2016	Start observing the cracks circumferentially, then the weld build-up and solution annealing were conducted as preventive actions.
2019	Observing the same crack trend, then replaced with a new primary reformer. The old samples that had been in service for 9 years were used in this work for assessment purposes.
2022	Once again, start observing the cracks circumferentially.

Table 2 Assessment in rating classes according to the results of the replica investigation

Rating ss	Structural or Damage Conditions	Limit Criteria
1	Creep-exposed, no creep pores	-
2a	Scattered creep pores	Up to 150 pores per mm^2
2b	Numerous creep pores, no orientation	More than 150 pores per mm^2
3a	Numerous creep pores with orientation	-
3b	Linear creep porosity, scattered grain boundary separations	At least 2 successive grain boundaries with at least 3 pores
4	Microcracks	More than one grain boundary length
5	Macrocracks	-

Notes: 150 pores per mm^2 correspond at 500 times magnification:
(i) Approx. 14 pores at a picture ratio of 13 x 18 cm or
(ii) Approx. 8 pores at a picture ratio of 10 x 14 cm
(iii) Approx. 5 pores at a picture ratio of 8 x 11 cm

3. RESULTS AND DISCUSSION

The physical conditions and laboratory results of the hot indication by the dye-penetrant method. Figures 1, 2, and 3 show the hot and cold collector weldolet from its collector weldolet are discussed. Four locations of circumferential cracks at the hot collector weldolet to outlet hairpin weldment were found with rejectable overview, general view, and schematic diagram.

Table 3 Assessment in rating classes according to the results of replica investigation (WELD)

Rating	Structural or Damage Conditions	Limit Criteria
A	No creep pores	-
B	Scattered creep pores	< 150 pores per mm2
C	Numerous creep pores with linear porosity	>150 pores per mm2
D	Microcracks	More than one grain boundary length
E	Macrocracks	Identifiable in MT Test

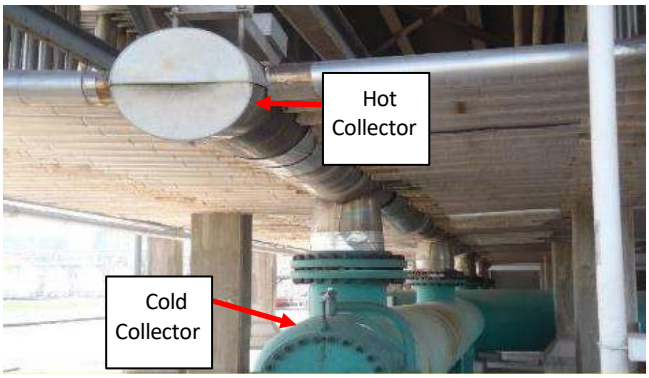

Figure 1. Overview of the hot and cold collector at the primary reformer.

Figure 2. General view of the outlet piping (hairpin) to weldolet (hot collector).

3.1 Chemical Composition Analysis

Chemical composition analysis was conducted on the weldolet in accordance with ASTM E415-17 [7]. The chemical composition results of the weldolet are tabulated in Table 4. The chemical composition of the weldolet complied with ASTM B408-22 for Alloy 800HT material specification [8]. The primary constituent elements of Incoloy/ Alloy 800HT are carbon, aluminium, and titanium. The carbon content in Incoloy 800H and 800HT results in high-temperature strength and resistance to creep and rupture. Incoloy 800H and 800HT products are solution annealed. When comparing Incoloy 800H and 800HT, one key distinction is the control over carbon content. Incoloy 800H limits the carbon content to a range of 0.05%–0.10%, which is more restrictive than the 0.10% maximum in the base Incoloy 800. Incoloy 800HT takes this further, tightening the carbon range to 0.06%–0.10%. This stricter control over carbon composition plays a crucial role in enhancing the performance of the alloys, particularly in high-temperature environments. Moreover, 800H and 800HT impose grain size limitations, an additional measure absents in Incoloy 800, further improving their mechanical properties.

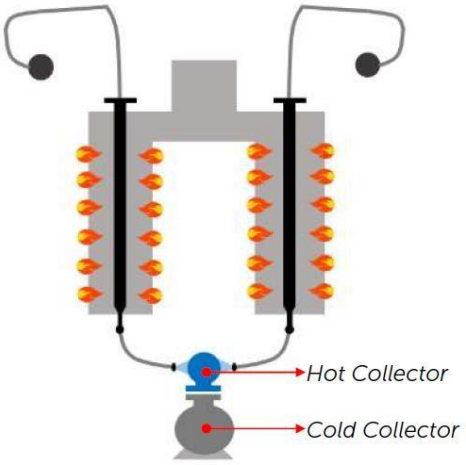

Figure 3. Schematic diagram of the hot and cold collector designed for side-firing and operating at temperature 910^{0}C for this work.

Table 4 Comparison of the chemical composition of the hot collector weldolet with the ASTM B408-22 standard

Element	ASTM B408-22 Requirement, %	Hot collector weldolet (Incoloy 800HT), %
C	0.06-1	0.07
Si	1.0 max	0.53
Mn	1.5 max	0.97
Cr	19-23	20.06
Mo	NA	0.22
Cu	0.75 max	0.32
Ni	30-35	30.81
Co	NA	0.09
Ti	0.15-0.6	0.59
Al	0.15-0.6	0.5
P	NA	0.02
S	0.015 max	0
Fe	39.5 min	45.6

Carbon increases mechanical properties such as strength, hardness, and mechanical resistance. The increase in the carbon content in the steel composition reduces the ductility of the material, which will cause it to show brittle properties. There is a risk of cracking in high- carbon steels due to residual austenite, which will occur after heat treatment. Aluminium is used as a deoxidiser in this case. It has a grain refinement feature, preventing the growth of austenite grains. This will also increase ageing resistance. Titanium improves strength and corrosion resistance while limiting austenite grain size. At 0.25-0.60 per cent titanium content, carbon combines with the titanium, allowing chromium to remain at grain boundaries and resist oxidisation. Chromium is the most used alloying element in steel. Chromium increases resistance to both corrosion and abrasion. Chromium steels maintain strength at elevated temperatures. A minimum amount of 20% Chromium content is needed sigma phase to occur. Sigma phase formation becomes increasingly challenging when the Chromium content falls below 20%. However, the inclusion of elements such as molybdenum, silicon, manganese, or nickel tends to lower this lower limit [9].

3.2 Visual and Dye Penetrant Testing Findings

Visual and dye penetrant testing examination accompanied by photographic documentation was performed on the four locations of circumferential cracks at the hot collector weldolet to outlet hairpin weldment. The general and close-up views after the dye penetrant testing are presented in Figures 1 to 9.

Figure 4 shows the hot collector weldolet of joint A with a linear circumferential crack of 10 mm, facing south and the location between 10 and 12 o'clock. While Figure 5 of joint B shows two different types of cracks. After the dye penetrant testing, cracks become obvious and indicate a rounded crack of 6 mm, facing south and the location at 3 o'clock, whilst the other one is a linear circumferential crack of 30 mm, facing south and the location at 12 o'clock.

(a) (b)

Figure 4. Hot collector weldolet of joint A, (a) general views and (b) showing linear circumferential crack of 10 mm.

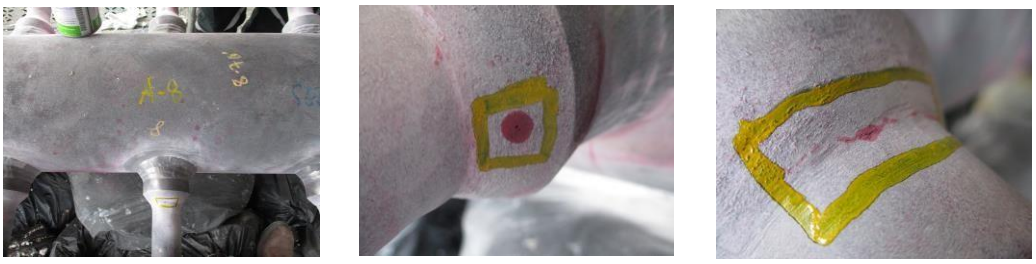

(a) (b) (c)

Figure 5. Hot collector weldolet of joint B, (a) general views, (b) showing the rounded crack of 6 mm and (c) with linear circumferential crack of 10 mm.

The third location of the circumferential crack was observed on the hot collector weldolet of joint C in Figure6. A rounded crack of 6 mm was found, it was facing south and the location at 12 o'clock. The fourth location was at joint D, as can be seen in Figure 7, where it appears to have a rounded crack of 6 mm, facing south and at 1 o'clock. In summary, rounded and linear circumferential cracks are the two types of cracks observed.

(a) (b)

Figure 6. Hot collector weldolet of joint C, (a) general views, (b) showing the rounded dye penetrant finding of 6 mm, facing south and the location at 12 o'clock.

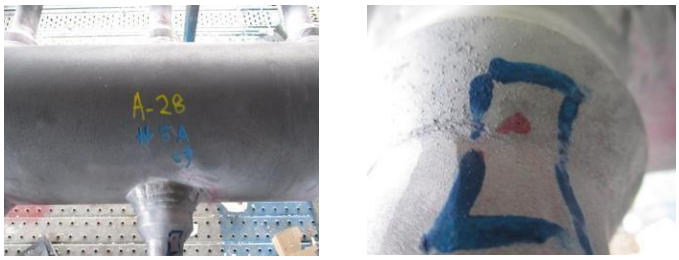

(a) (b)

Figure 7. Hot collector weldolet of joint D, (a) general views, (b) showing the rounded dye penetrant finding of 6 mm, facing south and the location at 1 o'clock.

3.3 In-situ Replication Findings

In-situ replication works were conducted on the hot collector weldolet to outlet hairpin weldment. Four locations were inspected, and the work was carried out on the weldment, which consisted of BM, HAZ and WELD. Table 5 provides detailed locations of the replication and hardness measurement on the weldolet.

Table 5 Location/ Joint of the replication and hardness measurement works on the weldolet

No	Location/ Joint	Material
1	A	Incoloy 800HT
2	B	
3	C	
4	D	

Microstructural images of joint A- hot collector weldolet were shown in Figure 8 where (a) BM, (b) HAZ and (c) WELD. The nature of the crack observed was an intergranular crack and can be observed in Figures 8-11. From the BM microstructural image, austenite grains were identified, and the creep cavity was not found. It was discovered that the sigma (σ) phase precipitates in the Cr-rich regions (α-Fe, ferrite). Chromium readily diffuses into α-Fe, functioning as a stabilizing element for the ferritic phase. Consequently, α-Fe serves as a favorable location for the precipitation of σ phase [10]. At the HAZ microstructural image, the fusion line was obviously seen, it separates the base metal and weld deposit regions. Austenite grains were clearly observed in the base metal regions with the α-Fe and σ phases. There is no sign of creep cavity found in the image (Figure 8(b)). Figure 8(c) shows the WELD microstructural images with no crack detected. It was only discovered the dendrites of austenite. Figure 9 is the microstructural images of Joint B- hot collector weldolet with (a) BM, (b) HAZ and (c) WELD. The crack detected at Joint B was categorized as intergranular crack. From the BM microstructural image, the austenite grains, α-Fe and σ phases were identified. While no creep cavity was found. The HAZ microstructural image as in Figure 9(b) shows a distinct fusion line that separates the base metal and weld deposit. α-Fe and σ phases were also detected, but no creep cavity was identified. At the same time, it was found that the dendrites of austenite, α-Fe and σ phases were observed from Figure 9(c) of the WELD microstructural images of Joint B- hot collector weldolet.

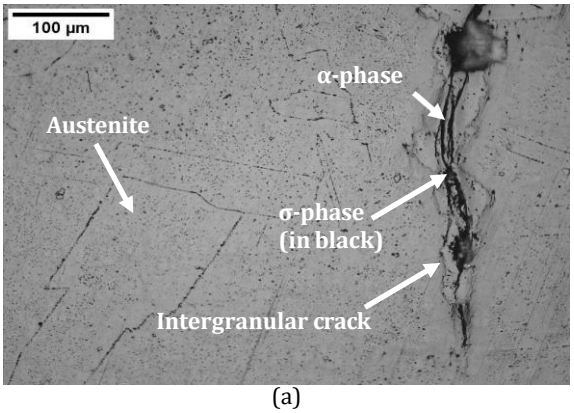

(a)

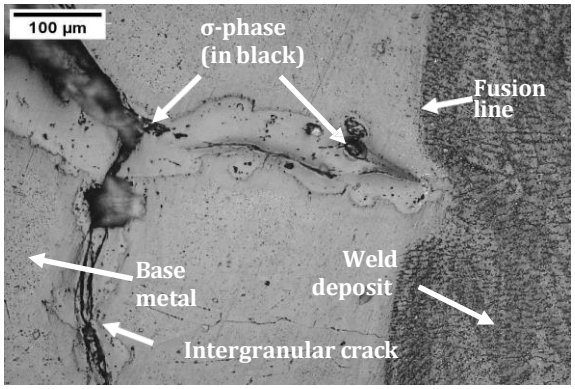

(b)

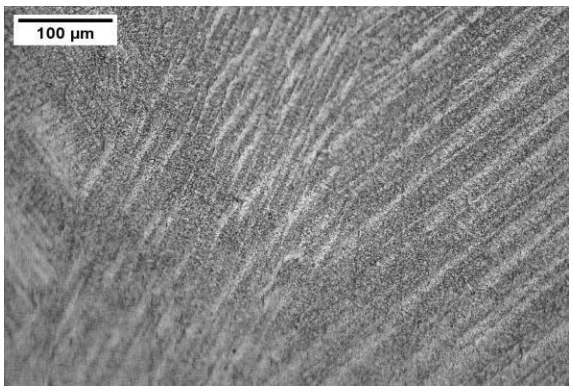

(c)

Figure 8 Microstructural images of hot collector weldolet of joint A where (a) BM, (b) HAZ and (c) WELD.

Microstructural images of hot collector weldolet at Joint C are shown in Figure 10. Figure 10(a) represents the BMimage with austenite grains, α-Fe and σ phases. In HAZ microstructural image as shown in Figure 10(b), the fusion line was clearly identified, and the weld deposit appears in a darker colour as compared to the base metal area. The α- Fe and σ phases were obviously shown. Concurrently, the WELD image (Figure 10(c)) shows the dendrites of austenite, together with the α-Fe and σ phases. It was determined that the creep cavity was not observed in all three welding regions.

Subsequently, Figure 11 denotes the microstructural images of hot collector weldolet at Joint D. BM image reveals the austenite grains, α-Fe and σ phases as shown in Figure 11(a). While the HAZ image identifies the α-Fe and σ phases with a clearly shown fusion line that separates the base metal and weld deposit regions as can be observed in Figure 11(b). Simultaneously, Figure 11(c) represents the WELD image which indicates the α-Fe and σ phases with the dendrites of austenite. There is no creep cavity found in all three welding regions.

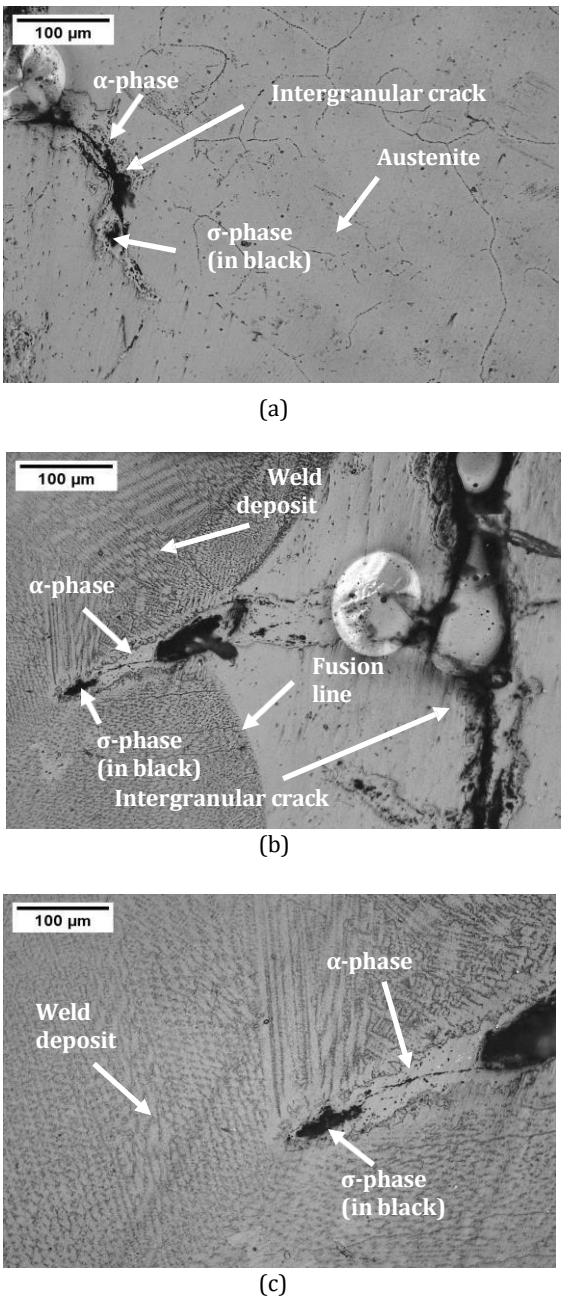

Figure 9 Microstructural images of hot collector weldolet of joint B where (a) BM, (b) HAZ and (c) WELD.

It can be concluded that the cracks detected were categorized as intergranular cracking. The weld and base metal regions were clearly seen with the fusion line in between those two regions. The HAZ microstructural images reveal a sensitization issue observed in the HAZ region, primarily attributable to the concentrated high heat input. Sensitization denotes a deterioration in corrosion resistance associated with the precipitation of Cr-rich carbides, for example, $M_{23}C_6$ and M_7C_3 along grain boundaries. While interstitial carbon can diffuse rapidly, chromium diffuses at a significantly slower rate. Consequently, this creates Cr-depleted zones adjacent to grain boundaries, brought about by the formation of chromium carbides that remove chromium from the solution. This chromium depletion renders the grain boundary area "sensitized," with the depleted region acting as anodic relative to the bulk material, resulting in accelerated corrosion along the grain boundaries.

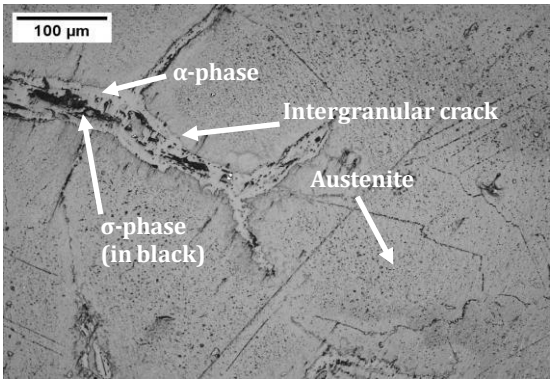

(a)

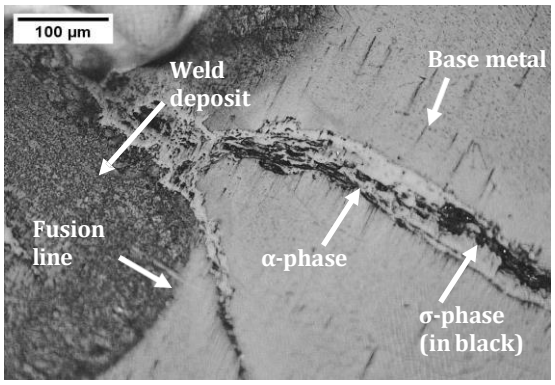

(b)

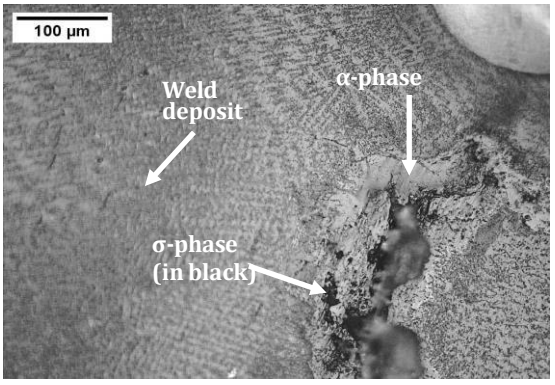

(c)

Figure 10. Microstructural images of hot collector weldolet of joint C where (a) BM, (b) HAZ and (c) WELD.

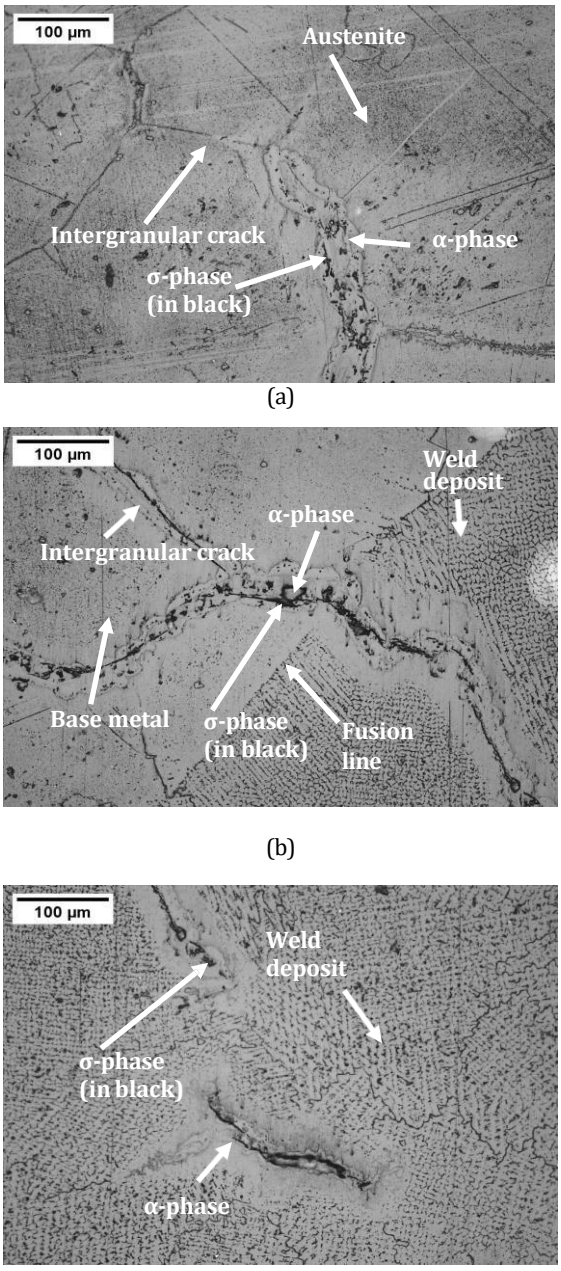

Figure 11. Microstructural images of hot collector weldolet of joint D where (a) BM, (b) HAZ and (c) WELD.

In situations where the alloy is exposed to an environment capable of attacking it, sensitization can lead to severe intergranular corrosion [11]. Thus, the observed damage mechanism of the crack was 'Aged Phenomenon', where the carbides are expected to undergo phase changes. Due to the aging process, there is a significant decrease in room temperature tensile elongation (strain at which failure occurs). This reduction becomes more pronounced as the exposure temperature increases. This diminished ductility increases the material's susceptibility to cracking due to the expansions and contractions that occur during the shutdown and startup of the reformer furnace [12].

The microstructure of the WELD indicates that the higher heat input during welding might be the cause for the formation of a harder dendritic structure, as the microstructure for WELD regions in all four joints showed dendritic structures, which were more prone to cracking.

Table 6 Summary of the microstructure, hardness and creep class/ratings on hot collector weldolet at different location/ joint

Location/ Joint	Microstructure	Average Hardness, HV (UCI)		Class Rating	Remark
A	Austenite grains with twins. Sigma phase was observed.	BM	194	1	Crack
	Fusion line between the base metal and the weld deposit. Sigma phase was observed.	HAZ	209	A	Crack
	Dendrites of austenite. Sigma phase was not observed.	WELD	235	A	No crack
B	Austenite grains with twins. Sigma phase was observed.	BM	193	1	Crack
	Fusion line between the base metal and the weld deposit. Sigma phase was observed.	HAZ	218	A	Crack
	Dendrites of austenite. Sigma phase was observed.	WELD	239	A	Crack
C	Austenite grains with twins. Sigma phase was observed.	BM	193	1	Crack
	Fusion line between the base metal and the weld deposit. Sigma phase was observed.	HAZ	219	A	Crack
	Dendrites of austenite. Sigma phase was observed.	WELD	243	A	Crack
D	Austenite grains with twins. Sigma phase was observed.	BM	194	1	Crack
	Fusion line between the base metal and the weld deposit. Sigma phase was observed.	HAZ	220	A	Crack
	Dendrites of austenite. Sigma phase was observed.	WELD	238	A	Crack

3.4 Vickers Hardness Measurement

On-site Vickers hardness measurements were conducted on the four different locations on the hot collector weldolet to outlet hairpin weldment. The hardness measurements were carried out on the weldment which consisted of BM, HAZ and WELD. The detailed locations of the replication and hardness measurement work on the weldolet can be referred in Table 5.

The structure of the weld zone clearly explains the variation in Vickers microhardness test results between BM, HAZ and WELD regions, as shown in Figure 12. The average hardness values of base metal were in the range of
187 HV up to 215 HV. This range indicates the base material's inherent hardness before any welding takes place. The heat-affected zone is the region surrounding the weld where the base metal has been subjected to high temperatures during welding but has not melted. The hardness values were measured between 200 HV and 222 HV in this area. The increase in hardness in the HAZ is primarily due to the thermal cycling and rapid heating and cooling experienced during welding. The weld deposit refers to the actual welded portion of the joint where filler material has been added to fuse the base metals together. Hardness values for the weld deposit were found to be in the range from 214 HV to 235 HV. The elevated hardness in this region is often a result of the solidification and cooling of the molten filler material, which can lead to the formation of harder microstructures. The hardness of the weld deposit is crucial because it influences the joint's overall strength and resistance to wear and fatigue. A summary of the microstructure, hardness and creep class/ratings on hot collector weldolet at different locations is shown in Table 6.

3.5 Rectification Measures

The first step in the rectification process involves heat treatment. It is specifically recommended and feasible to implement a solution annealing process which entails heating the affected components to a temperature of 1150^0C and holding them at this temperature for a minimum of one hour. This extended exposure to high heat breaks down and dissolves any existing sigma phase formations within the material. Sigma phase is an intermetallic compound that can negatively affect the material's mechanical properties and corrosion resistance. After the one-hour hold, the rapid cooling of the material is achieved using forced air. This cooling process is essential to maintain the desired microstructure and prevent the reformation of sigma phase. Once this heat treatment is completed, the material should have improved mechanical and corrosion resistance properties.

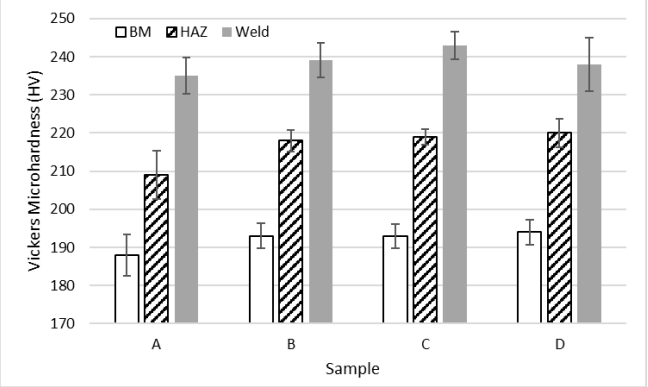

Figure 12. Vickers microhardness test results on hot collector weldolet of joints A, B, C and D at three different welding zones.

After the heat treatment, the next step is to address any cracks that may have formed in the material. This is achieved through light grinding to remove the surface imperfections caused by the cracks. Following the grinding process, a thorough inspection is conducted using DPT to ensure that all cracks have been adequately removed and there are no remaining defects. If any defects or cracks are still present, they should be addressed before proceeding further.

Once the material is free from cracks and defects, the next step is to rebuild any lost material through welding. This process involves depositing additional weld material onto the affected areas to restore them to their original dimensions and strength. The welding process should be carried out meticulously to ensure proper fusion and the absence of any new defects.

After the welding and repair work is completed, a final series of inspections and tests are performed to ensure the quality and integrity of the repaired component. This includes:

- Visual inspection: A visual examination of the repaired areas to check for any visible defects, irregularities, or signs of incomplete welding.
- DPT: Another round of DPT is conducted to confirm that the welding and repair work did not introduce any new defects, such as cracks or discontinuities.
- Hardness test: A hardness test is carried out to assess the material's mechanical properties and ensure that they meet the specified requirements.
- Ultrasonic testing for flaws (UTFD) and phased array ultrasonic testing (PAUT): UTFD uses ultrasonic waves to detect any internal flaws or defects within the material, ensuring that it is free from hidden defects. PAUT in weldment inspections arises from its advanced UT technique capabilities, including precise scanning, improved resolution, and real-time imaging with electronically controlled ultrasonic elements, alongside automated scanning systems, collectively enhancing weld reliability and safety in critical industries. PAUT's efficiency and accuracy can lead to cost savings in terms of labour and equipment, as it can reduce the need for extensive rework or repairs due to undetected defects.

By following these four comprehensive steps, the issue regarding the sigma phase formation can be rectified, and cracks and defects in the material can, ultimately restoring it to its intended performance and safety standards. It is crucial to conduct these steps carefully and in accordance with relevant industry standards and procedures to ensure the effectiveness of the rectification process.

4. CONCLUSION

The microstructures of the BM of outlet hairpin for all the locations inspected consist of austenite grains. HAZs for all the locations analysed consist of fusion line with no clear HAZ regimes (coarse-grained HAZ, fine-grained HAZ and intercritical HAZ) due to the material's thermal conductivity. The microstructure for weld deposit is dendrites of austenite which was formed as the result of solidification of filler metal during welding. Creep cavity/pore was not observed; hence, these locations are classified as Class 1 for the BM, Class A for the HAZ and the weld deposit according to VGB Standard [6].

σ-phase was observed in the microstructure in the base metal as well as weld deposit except for location A1-Weld deposit as shown in Figure 8(c). Intergranular cracks were observed adjacent to σ-phase. The inspected locations were classified as Class 1 for the base metal and Class A for

HAZ and weld deposit even though cracks were observed at these locations because creep pore/cavity was not observed, and the cracking was not due to creep but probably due to sigma phase embrittlement.

More cracks were observed in the base metal than in other locations. Overall, the Vickers microhardness test results increased from BM to HAZ to WELD with no significant differences.

ACKNOWLEDGEMENTS

The author would like to express gratitude and appreciation to the technical support from our industry partner (which has to undisclosed their names) and academic support from the Faculty of Chemical Engineering and Technology, Universiti Malaysia Perlis (UniMAP), for their involvement in the research. This research was funded and supported under grant number FRGS/1/2020/STG05/UNIMAP/02/3 by the Fundamental Research Grant Scheme (FRGS) from the Ministry of Education Malaysia.

REFERENCES

[1] J. Swaminathan, Raghubir Singh, Swapan Kumar Das and Goutam Das (2006). Failure Analysis of Welded Reformer Tubes of a Fertilizer Unit in Proceeding of the International Conference & Exhibition on Pressure Vessels and Piping, "OPE 2006 –CHENNAI", Chennai, India.

[2] Bhupendra Gaur (2017). Damage analysis and integrity assessment of a few steam-reformer components at a syn-gas plant, Mechanics & Industry 18, 401.

[3] G. N. Haidemenopoulos, K. Polychronopoulou, A. D. Zervaki, H. Kamoutsi, S. I. Alkhoori, S. Jaffar, P. Cho, and H. Mavros (2019). "Aging Phenomena during In- Service Creep Exposure of Heat-Resistant Steels," Metals, vol. 9, p. 800.

[4] C. Maharaj, A. Marquez and R. Khan (2019). "Failure Analysis of Incoloy 800HT and HP-Modified Alloy Materials in a Reformer," Journal of Failure Analysis and Prevention, 19, p. 291–300.

[5] ASTM. "ASTM E1351-01 (2020): Standard Practice for Production and Evaluation of Field Metallographic Replicas." ASTM International, 2020.

[6] VGB PowerTech. "VGB-S-517-00-2014-11-DE-EN: Inspection of Boiler Components Using Borescopes - Part 1: Borescope." VGB PowerTech, 2014.

[7] ASTM. "ASTM E415-17: Standard Test Method for Analysis of Carbon and Low-Alloy Steel by Spark Atomic Emission Spectrometry." ASTM International, 2017.

[8] ASTM. "ASTM B408-22: Standard Specification for Nickel-Iron-Chromium Alloy Rod and Bar." ASTM International, 2022.

[9] D. Herring, "Sigma Phase Embrittlement," Industrial heating, www.industrialheating.com, Accessed date 4th October 2023, 2012.

[10] D. D. S. Silva, T. A. Simões, D. A. Macedo, A. H. S. Bueno, S. M. Torres, and R. M. Gomes, "Microstructural influence of sigma phase on pitting corrosion behavior of duplex stainless steel/NaCl electrolyte couple," *Materials Chemistry and Physics*, vol. 259, p. 124056, 2021.

[11] S. Arun Kumar and P. Sathiya, "Effects of Heat Input on the Mechanical and Metallurgical Characteristics of TIG Welded Incoloy 800HT Joints," *Archives of Metallurgy and Materials*, vol. 62, no. 3, pp. 1673-1679, 2017.

[12] G. N. Haidemenopoulos, K. Polychronopoulou, A. D. Zervaki, H. Kamoutsi, S. I. Alkhoori, S. Ja ar, P. Cho, and H. Mavros, "Aging Phenomena during In-Service Creep Exposure of Heat-Resistant Steels," *Metals*, vol. 9, no. 7, p. 800, 2019, doi: 10.3390/met9070800.